Snapshots of a Dynamic Folding Nucleus in Zinc-Substituted *Pseudomonas aeruginosa* Azurin†

Corey J. Wilson‡,§ and Pernilla Wittung-Stafshede*,‡,§,||

Department of Biochemistry and Cell Biology, Keck Center for Structural Computational Biology, and Department of Chemistry, Rice University, 6100 Main Street, Houston, Texas 77251

Received February 23, 2005; Revised Manuscript Received June 13, 2005

ABSTRACT: Zinc-substituted *Pseudomonas aeruginosa* azurin folds in two-state equilibrium and kinetic reactions. In the unfolded state, the zinc ion remains bound to the unfolded polypeptide via two native-state ligands (His117 and Cys112). The significantly curved Chevron plot for zinc-substituted azurin was earlier ascribed to movement of the folding-transition state. At low concentrations of denaturant, the transition state occurs early in the folding reaction (low Tanford β-value), whereas at high-denaturant concentration, it moves closer to the native structure (high Tanford β-value). Here, we use this movement to track the formation and growth of zinc-substituted azurin's folding nucleus with atomic resolution using protein engineering. The average phi (ϕ) value for 17 positions (covering all secondary-structure elements) goes from 0.25 in 0 M GuHCl ($\beta \sim 0.46$) to 0.76 in 4 M GuHCl ($\beta \sim 0.86$); a ϕ-value of 1 or 0 indicates native-like or unfolded-like interactions, respectively. Analysis of individual ϕ-values reveals a delocalized nucleus where structure condenses around a leading density centered on Leu50 in the core. The diffuse moving transition state for zinc-substituted azurin is in sharp contrast to the fixed polarized folding nucleus observed for apo-azurin. The dramatic difference in apparent kinetic behavior for the two forms of azurin can be rationalized as a minor alteration on a *common* free-energy profile that exhibits a broad activation barrier.

Many proteins fold spontaneously in vitro, but the mechanisms of such processes are not fully understood. Small, single-domain proteins often fold by two-state equilibrium and kinetic mechanisms (*1*, *2*). For such proteins, three states are important for defining kinetic and thermodynamic behavior: the native, transition, and denatured states. The transition state consists of a set of structures (i.e., the transition-state ensemble), whose formation is rate-limiting for folding of the native state from the denatured ensemble. As the transition state never accumulates, details about its properties must be inferred indirectly (*3*). The protein engineering approach has proven to be the most important experimental strategy for obtaining specific information about interactions between residues in the transition state (*4*, *5*). In such experiments, structure in the transition state is probed by measuring the kinetic and thermodynamic effects of mutations in different regions of the protein. The results are typically presented as ϕ-values, which represent the change in stability of the transition state accompanying the mutation of a residue relative to the effect of the same mutation in the native state. Thus, ϕ equal to 1 suggests that a residue is found in a highly structured region of the transition state and makes interactions that contribute equally to the stability of the transition and the native states. In contrast, ϕ equal to 0 indicates that the residue forms very few, if any, interactions with other residues in the transition state. Fractional ϕ-values may be interpreted as possessing different degrees of structure in the folding nucleus (*6*, *7*).

Several small proteins folding by two-state kinetic mechanisms have been subjects of mutagenesis to obtain a picture of the folding transition state with residue-specific resolution. The results of these studies have led to the distinction of two classes of folding-transition states, namely diffuse and polarized transition states (*8*, *9*). In diffuse transition states, all but a few side chains have similar ϕ-values, which are relatively low. This has been shown to indicate a nucleation−condensation mechanism with the folding nucleus located diffusively around a few side chains with particularly high ϕ-values (e.g., CI2[1], Arc repressor, CheY, and λ repressor (*9*−*12*)). In contrast, polarized transition states display distinct substructures that have much higher ϕ-values than the rest of the protein, wherein ϕ-values are approximately zero (e.g., ACBP, fyn SH3, Im7, protein L, and src SH3 (*13*−*17*)).

Chevron plots (i.e., logarithms of rate constants versus denaturant concentration) are normally V-shaped for two-state proteins. This classic V-shape is indicative of a fixed transition-state position relative to the unfolded and folded

† Support for this project was provided by grants from NIH (GM059663) and the Robert A. Welch Foundation (C-1588). C.J.W. is supported by the Houston Area Molecular Biophysics Program (GM08280).

* Corresponding author. E-mail, pernilla@rice.edu; phone, 713-348-4076; fax, 713-348-5154.

‡ Department of Biochemistry and Cell Biology.

§ Keck Center for Structural Computational Biology.

|| Department of Chemistry.

[1] Abbreviations: GuHCl, guanidine hydrochloride; CD, circular dichroism; CI2, chymotrypsin inhibitor 2; U, unfolded state; N, native state.

10.1021/bi050342n CCC: $30.25
Published on Web 07/08/2005

structures; moreover, the relative position of the transition state is given by the Tanford β-value (*18*, *19*). In recent years, it has been observed that some proteins exhibit curved Chevron plots (i.e., β changes as a function of denaturant concentration). In general, this may be a result of (i) a change in the rate-limiting step on a sequential pathway, (ii) a change in the mechanism of the reaction due to a switch between parallel pathways, (iii) structural changes in the ground state(s), (iv) a movement of the position of the transition state along a broad barrier, or (v) transient protein aggregation (*20*−*22*). In pioneering work, Oliveberg et al. showed that the symmetrical curvature in the Chevron plot for the protein U1A was the result of transition-state movement. Despite the curvature, the kinetic folding mechanism remained two-state (*23*−*26*). When the transition-state movement is used, the growth of the U1A's folding nucleus could be analyzed with residue-specific resolution using ϕ-value analysis (*25*). It was found that the U1A's transition state was delocalized and consolidated in a typical nucleation−condensation pattern. Evidence for transition state movement has also been observed upon point mutations in the structurally homologous proteins CI2 and S6 (*24*). This behavior is also proposed by theory and simulations in which the kinetic bottleneck changes location in the folding funnel upon alterations of the protein's stability (*10*, *27*−*31*).

Pseudomonas aeruginosa azurin is a small (128 residues) single-domain protein with a β-barrel structure composed of eight β-strands, which belongs to the sandwich-like protein family (*32*). In vivo, a redox-active copper is coordinated to the protein allowing for electron-transfer activity (*32*). The copper in azurin can be eliminated, creating apo-azurin, or substituted for zinc without change of the overall structure (*33*, *34*). Equilibrium and kinetic folding processes for apo-azurin are two-state reactions (*35*−*39*). In terms of exposed hydrophobic surface area, apo-azurin folds via a 60% native-like transition-state (i.e., $\beta \sim 0.6$) with a speed that is in excellent agreement with the predicted value based on the native-state topology (*35*, *36*, *40*, *41*). Recently, apo-azurin's folding-transition state was probed by protein engineering. The focus was on core residues found to be structural determinants in 94% of all sandwich-like proteins (*42*). The folding nucleus appeared to be highly polarized; that is, a few core residues had ϕ-values of 1, whereas others had low ϕ-values (*43*).

Zinc-substituted *P. aeruginosa* azurin also folds in two-state equilibrium- and kinetic reactions (*38*, *44*). It has been demonstrated that zinc remains bound to zinc-substituted azurin when unfolded by guanidine hydrochloride (GuHCl) via the side chains of residues Cys112 and His117 (*45*). In sharp contrast to apo-azurin, the Chevron plot for zinc-substituted azurin exhibits curvature in both folding and unfolding limbs. On the basis of extensive investigations, we concluded that this behavior was not due to transient aggregation or transient intermediates. Rather, the curvature is a result of transition-state movement as a function of denaturant concentration within a two-state kinetic mechanism (*38*). Here, we use ϕ-value analysis to obtain snapshots of zinc-substituted azurin's dynamic folding nucleus with residue-specific resolution. Analysis of 17 point-mutated variants of zinc-substituted azurin, covering all secondary-structure elements, reveals that the folding nucleus is delocalized and gradually grows more native-like around a center density situated on Leu50. The dramatic difference in kinetic-folding behavior between apo- and zinc-forms of azurin is rationalized in terms of small changes on a *common* broad activation barrier.

MATERIALS AND METHODS

Construction of Variants. A pUC18 vector containing the wild-type *P. aeruginosa* azurin gene was used as the template to create the point-mutated variants (i.e., Val5Ala, Ile7Ala, Ile20Ala, Val22Ala, Val31Ala, Leu33Ala, Trp48Ala, Leu50Ala, Val60Ala, Ile81Ala, Ala82Gly, Val95Ala, Phe97Ala, Tyr108Ala, Phe110Ala, Met121Ala, and Ile125Ala azurin) via QuickChange site-directed mutagenesis as reported in refs *43* and *45*. Variants were expressed in *Escherichia coli* BL21pLysS cells, and purification was performed as in ref *37*. To ensure 100% zinc-substitution, the apo-form of each variant was first prepared by extensive cyanide dialysis (to remove both copper and zinc), followed by a subsequent dialysis in the presence of excess zinc. Successful zinc-reconstitution was verified by copper-titration monitoring absorption at 630 nm (*37*).

Equilibrium Unfolding. GuHCl-induced equilibrium unfolding was performed in 100 mM Tris-HCl, pH 7.0, at 25 °C, using fluorescence (excitation at 285 nm; emission monitored at 308 nm) and far-UV circular dichroism (CD) detection (200−300 nm). Samples were incubated for 2 h before measurements. The equilibrium-unfolding reactions were reversible without any display of protein-concentration dependence (in 5−50 μM protein range). For the Trp48Ala variant, tyrosine fluorescence was used in combination with far-UV CD. The equilibrium-unfolding curves for wild-type and mutant zinc-substituted azurins were analyzed using a two-state model (*46*, *47*) to determine $\Delta G_U(H_2O)$ and m_{F-U} values. The transition-midpoints were calculated as $\Delta G_U(H_2O)/m_{F-U}$ and by direct inspection of the transitions. For each apo-azurin variant, far-UV CD- and fluorescence-detected transitions overlapped. The $\Delta G_U(H_2O)$ values listed in Table 1 are average values from fits to both CD and fluorescence curves. Errors (standard deviations) are derived from multiple experiments.

Folding Dynamics and Data Analysis. Time-resolved folding and unfolding was probed by fluorescence (excitation at 285 nm; emission monitored at 308 nm) and far-UV CD (at 220 nm) using an Applied Photophysics Pi-Star stopped-flow mixer. Both detection modes gave identical kinetic traces in all cases. Zinc-substituted azurin variants were mixed in 1:10 ratio with appropriate GuHCl/buffer solutions. Six kinetic traces were averaged and fit to monophasic decay equations for unfolding and biphasic decay equations for refolding. There were no missing amplitudes (within the 2−3 ms dead time) in either fluorescence or far-UV CD kinetic traces, and no protein-concentration dependence was found (in the 5−50 μM protein range tested). For each variant, the minor slow refolding phase (less than 15% of fluorescence and far-UV CD signal changes in all cases) was neglected in this study. Unfolding and refolding (i.e., the fast, major phase) rate constants at different GuHCl concentrations were fit to second-order polynomials (*24*, *25*):

$$\ln k_{obs} = \ln[k_F(H_2O)\exp(b_F[\mathrm{GuHCl}] + c_F[\mathrm{GuHCl}]^2) + k_U(H_2O)\exp(b_U[\mathrm{GuHCl}] + c_U[\mathrm{GuHCl}]^2)] \quad (1)$$

Table 1: Thermodynamic and Kinetic Parameters for Wild-Type and Point-Mutated Zinc-Substituted Azurin Variants in the Absence of Denaturant (pH 7, 25 °C)[a]

azurin variant	$\Delta G_U(H_2O)$ (kJ/mol)	$\Delta\Delta G_U(H_2O)$ (kJ/mol)	m_{U-F} (kJ/mol,M)	$k_F(H_2O)$ (s^{-1})	$\Delta\Delta G^{\ddagger}(H_2O)$ (kJ/mol)	$\beta(H_2O)$	$\phi(H_2O)$[b]
wild-type	54 ± 1.5	-	17 ± 1.5	126 ± 18	-	0.41 ± 0.08	-
Val5Ala	50 ± 1	−4 ± 1.5	17 ± 1.5	99 ± 9	−0.6 ± 0.3	0.38 ± 0.10	0.15 ± 0.09
Ile7Ala	40 ± 1	−14 ± 1.5	18 ± 1.5	81 ± 5	−1.1 ± 0.3	0.39 ± 0.10	0.08 ± 0.02
Ile20Ala	44 ± 1.5	−10 ± 1.5	19 ± 1.5	69 ± 6	−1.5 ± 0.3	0.56 ± 0.06	0.15 ± 0.04
Val22Ala	47 ± 1	−7 ± 1.5	19 ± 1.5	84 ± 7	−1.0 ± 0.3	0.47 ± 0.10	0.14 ± 0.05
Val31Ala	47 ± 1	−7 ± 1.5	19 ± 1.5	42 ± 3	−2.7 ± 0.3	0.56 ± 0.06	0.39 ± 0.09
Leu33Ala	47 ± 1	−7 ± 1.5	20 ± 1.5	55 ± 4	−2.0 ± 0.3	0.56 ± 0.06	0.29 ± 0.06
Trp48Ala	40 ± 1.5	−14 ± 1.5	20 ± 1.5	22 ± 2	−4.2 ± 0.3	0.47 ± 0.05	0.30 ± 0.04
Leu50Ala	46.5 ± 1	−7.5 ± 1.5	18.5 ± 1.5	32 ± 3	−3.3 ± 0.7	0.33 ± 0.07	0.44 ± 0.10
Val60Gly	41 ± 1	−13 ± 1.5	17.5 ± 1.5	50 ± 10	−2.3 ± 0.3	0.37 ± 0.07	0.18 ± 0.03
Ile81Ala	48 ± 1	−6 ± 1.5	20 ± 1.5	55 ± 7	−2.0 ± 0.3	0.58 ± 0.11	0.33 ± 0.09
Ala82Gly	47 ± 1	−7 ± 1.5	18 ± 1.5	45 ± 7	−2.5 ± 0.3	0.36 ± 0.10	0.36 ± 0.08
Val95Ala	50 ± 1	−4 ± 1.5	18 ± 1.5	67 ± 8	−1.5 ± 0.3	0.34 ± 0.08	0.38 ± 0.12
Phe97Ala	43 ± 1	−11 ± 1.5	20.5 ± 1.5	49 ± 7	−2.3 ± 0.3	0.55 ± 0.11	0.21 ± 0.04
Tyr108Ala	39 ± 1	−15 ± 1.5	18.5 ± 1.5	16 ± 3	−5.0 ± 0.3	0.50±0.10	0.33 ± 0.04
Phe110Ala	33 ± 1	−21 ± 1.5	19 ± 1.5	83 ± 5	−1.0 ± 0.3	0.31 ± 0.03	0.05 ± 0.02
Met121Ala	42 ± 1	−12 ± 1.5	17.5 ± 1.5	96 ± 6	−0.7 ± 0.2	0.26 ± 0.10	0.06 ± 0.03
Ile125Ala	47 ± 1	−7 ± 1.5	19 ± 1.5	44 ± 6	−2.6 ± 0.3	0.42 ± 0.10	0.36 ± 0.08
average			18.6 ± 1.5			0.46 ± 0.14	0.25 ± 0.12

[a] The ϕ-values are calculated as $\phi = \Delta\Delta G^{\ddagger}(H_2O)/\Delta\Delta G_U(H_2O)$, where $\Delta\Delta G_U(H_2O)$ is calculated as $\Delta G_U(\text{mutant},H_2O) - \Delta G_U(\text{wild-type},H_2O)$ and $\Delta\Delta G^{\ddagger}(H_2O)$ as $RT \ln[k_f(\text{mutant},H_2O)/k_f(\text{wild-type},H_2O)]$. The β-values are calculated according to eq 3 (Materials and Methods). Unless noted, errors are derived from the goodness of the appropriate fits. [b] Standard deviations (σ) for the ϕ-values were calculated as in ref *7*: $\sigma_\phi = |\phi| \cdot \sqrt{[(\sigma_{\Delta\Delta G^{\ddagger}}/\Delta\Delta G^{\ddagger})^2 + (\sigma_{\Delta\Delta GU}/\Delta\Delta G_U)^2]}$.

In this equation, b_F/b_U is the linear dependence of folding/unfolding and c_F/c_U is the parameter (a constant) describing the curvature observed in the folding/unfolding limbs in the Chevron plots; $k_F(H_2O)$ and $k_U(H_2O)$ are the folding and unfolding rate constants in aqueous solution (i.e., in the absence of GuHCl). The actual *m*-values (m_F/m_U) are given by the relationship:

$$m_F = \delta(\ln k_F)/\mathrm{d}[\mathrm{GuHCl}] = b_F + 2c_F[\mathrm{GuHCl}] \quad (2a)$$

$$m_U = \delta(\ln k_U)/\mathrm{d}[\mathrm{GuHCl}] = b_U + 2c_U[\mathrm{GuHCl}] \quad (2b)$$

The Tanford β-value for folding, which assesses the position of the transition state in relation to the folded and unfolded structures (*18*, *19*), is calculated as

$$\beta = -m_F/m_{F-U} = 1 - m_U/m_{F-U} \quad (3)$$

Thus, for curved Chevrons, β becomes a linear function of the denaturant concentration. A structural interpretation of β is the solvent exposure of the transition state relative to that of the native state.

RESULTS

Equilibrium Stability of Zinc-Substituted Azurin Variants. Past biophysical studies have demonstrated that zinc-substituted *Pseudomonas aeruginosa* azurin folds in two-state equilibrium- and kinetic reactions (*38*, *41*, *45*). The folding dynamics of zinc-substituted azurin exhibits curvature in both folding and unfolding limbs, when the natural logarithms of the observed rate constants are plotted as a function of GuHCl concentration. This curvature in the Chevron plot has been assigned to transition-state movement (*38*, *41*). Here, we take advantage of this behavior to investigate the folding-transition state of zinc-substituted azurin with residue-specific resolution. For this purpose, 17 point-mutated variants were created: Val5Ala, Ile7Ala, Ile20Ala, Val22Ala, Val31Ala, Leu33Ala, Trp48Ala, Leu50Ala, Val60Ala, Ile81Ala, Ala82Gly, Val95Ala, Phe97Ala, Tyr108Ala, Phe110Ala, Met121Ala, and Ile125Ala azurin. This selection involves two residues in seven of azurin's eight β-strands, one residue in the last β-strand, one residue in the α-helix, and one residue in a loop-region; together, the mutations probe all of azurin's secondary-structure elements. The zinc-forms of all the variants adopted folded structures that are essentially identical to wild-type azurin as deduced from their far-UV circular dichroism (CD) and tryptophan (Trp48) emission (except Trp48Ala variant) spectra (data not shown).

The thermodynamic stability of the zinc-form of each azurin variant was tested by guanidine hydrochloride (GuHCl) titrations monitored by far-UV CD and fluorescence. Like wild-type zinc- and apo-forms of azurin (*35*, *37*−*41*, *45*, *48*), the variants unfold in single, reversible transitions (Figure 1A). Curves derived from CD and fluorescence data are coincidental for each protein, which is indicative of two-state equilibrium-unfolding processes. The thermodynamic stability is lower for all the variants as compared to the stability of wild-type zinc-substituted azurin (Table 1). The most dramatic reduction in stability is found for the Phe110Ala azurin variant. In accord, this residue is situated near the zinc-binding site; therefore, by its elimination, the stabilizing effect of the zinc ion may be less efficiently transmitted throughout the overall structure. We note that the thermodynamic stability for wild-type zinc-substituted azurin reported here is somewhat higher than previous estimates (*38*, *45*). We have repeated our experiments manifold, and they are consistent. Thus, we tentatively ascribe this difference to solution conditions and the method of preparation of zinc-substituted azurin. Nonetheless, only differences in stability are important in this study. Moreover, the thermodynamic stability that is derived from the folding and unfolding kinetics for wild-type zinc-substituted azurin is within 15% of the obtained equilibrium-stability value.

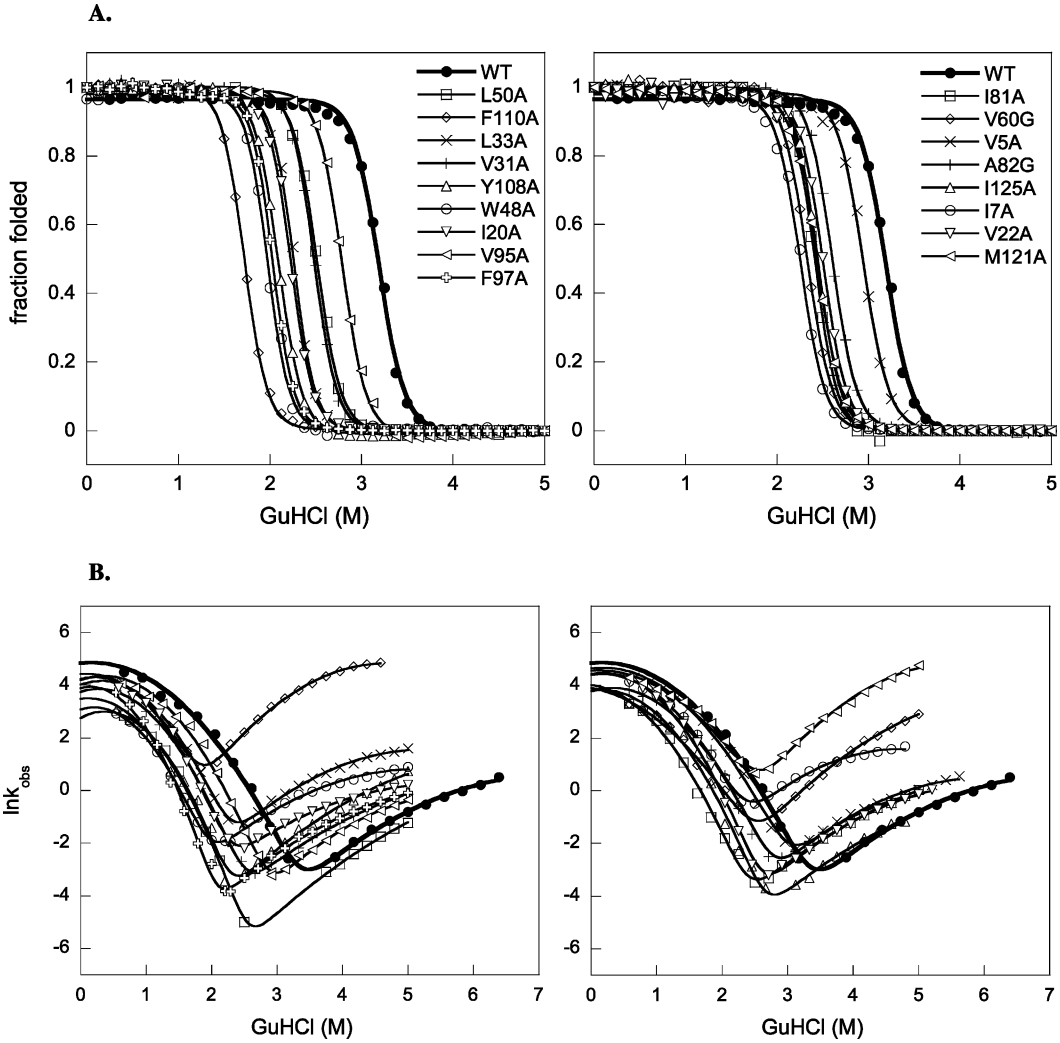

FIGURE 1: (A) GuHCl-induced equilibrium unfolding of wild-type and the 17 variants of zinc-substituted azurin (displayed in two figures for clarity). For each protein, CD- and fluorescence-detected transitions overlap (normalized fluorescence data shown). Solid curves are two-state fits to each set of data (Table 1). Legend to symbols is given in the figures. (B) Semilogarithmic graph of ln k_{obs} versus GuHCl for wild-type and the 17 variants of zinc-substituted azurin (displayed in two figures for clarity). Solid lines are polynomial fits to the data (see Materials and Methods). The symbol for each kinetic plot corresponds to the same symbol in the equilibrium plot directly above in Figure 1A.

Folding Dynamics of Zinc-Substituted Azurin Variants. Folding and unfolding kinetics of the variants were probed by fluorescence and far-UV CD detection methods using stopped-flow mixing (Figure 1B). As noted for wild-type zinc-substituted azurin (*38*), the unfolding processes are single-exponential decays, whereas the folding reactions are best fit with two exponentials. This was explained by the presence of two unfolded-state populations differing in their zinc coordination (*38*). The same bi-phasic folding behavior is observed for all variants studied here (data not shown). Since the faster of the two phases is dominant, including more than 85% of the fluorescence and far-UV CD amplitudes, this is the only phase we consider here. In support of two-state reactions (i.e., neglecting the minor slow-folding population), all kinetic traces were single-exponential decays and devoid of missing amplitude at all reported GuHCl concentrations. The latter observation is consistent with the lack of transient (i.e., burst-phase) intermediates within the stopped-flow dead time. For each variant, CD- and fluorescence-detected kinetic traces overlap at each condition. Moreover, there is no protein-concentration dependence in either unfolding or refolding phases, which rules out transient aggregation during the folding event. Still, for all zinc-azurin variants, the Chevron plots are curved (Figure 1B). In analogy with wild-type zinc-substituted azurin, this behavior is assigned to transition-state movement.

All Chevron plots were fit to second-order polynomials (eq 1 in Materials and Methods) to obtain folding- and unfolding-rate constants in water (Table 1). The β values at three selected GuHCl concentrations (calculated from the polynomial-fit parameters b_U and c_U and eqs 2b and 3 in Materials and Methods) are listed in Table 2; it is clear that similar transition-state movements occur for all zinc-substituted azurin variants. The thermodynamic stability derived from the kinetics and from the equilibrium experiments agree within 15% for all variants (data not shown). We have consistently used the thermodynamic stability derived from the equilibrium experiments in the ϕ-value analyses in this study.

Transition-State Movement and Free-Energy Profile for Wild-Type Zinc-Azurin. The curvatures in the Chevron plots imply that m_F grows larger while m_U decreases when the GuHCl concentration is increased. In all variants here, the increase in m_F roughly matches the decrease in m_U (i.e., c_F

Table 2: Residue-Specific Analysis of Zinc-Substituted Azurin's Folding-Transition State as a Function of Denaturant (0, 2, and 4 M GuHCl; pH 7, 25 °C)[a]

azurin variant	location of mutation	β (0 M)	β (2 M)	β (4 M)	ϕ (0 M)[b]	ϕ (2 M)[b]	ϕ (4 M)[b]
wild-type		0.41 ± 0.08	0.58 ± 0.08	0.76 ± 0.08	-	-	-
Val5Ala	strand 1	0.38 ± 0.10	0.59 ± 0.10	0.81 ± 0.10	0.15 ± 0.09	0.25 ± 0.10	0.33 ± 0.12
Ile7Ala	strand 1	0.39 ± 0.10	0.65 ± 0.10	0.90 ± 0.10	0.08 ± 0.02	0.24 ± 0.04	0.55 ± 0.06
Ile20Ala	strand 2	0.56 ± 0.07	0.74 ± 0.07	0.88 ± 0.07	0.15 ± 0.04	0.46 ± 0.06	**0.82 ± 0.09**
Val22Ala	strand 2	0.47 ± 0.10	0.64 ± 0.10	0.81 ± 0.10	0.14 ± 0.05	0.50 ± 0.09	**0.88 ± 0.10**
Val31Ala	strand 3	0.56 ± 0.06	0.73 ± 0.06	0.88 ± 0.06	0.39 ± 0.09	**0.67 ± 0.10**	**0.88 ± 0.09**
Leu33Ala	strand 3	0.56 ± 0.06	0.71 ± 0.06	0.81 ± 0.06	0.29 ± 0.06	0.39 ± 0.06	**0.69 ± 0.06**
Trp48Ala	strand 4	0.47 ± 0.05	0.69 ± 0.05	0.77 ± 0.05	0.30 ± 0.04	0.55 ± 0.06	**0.79 ± 0.06**
Leu50Ala	strand 4	0.33 ± 0.07	0.55 ± 0.07	0.76 ± 0.07	0.44 ± 0.10	0.97 ± 0.15	**1.04 ± 0.12**
Val60Gly	helix	0.37 ± 0.07	0.55 ± 0.07	0.74 ± 0.07	0.18 ± 0.03	0.36 ± 0.06	0.51 ± 0.08
Ile81Ala	strand 5	0.58 ± 0.11	0.69 ± 0.11	0.79 ± 0.11	0.33 ± 0.09	**0.75 ± 0.12**	**0.89 ± 0.10**
Ala82Gly	strand 5	0.36 ± 0.10	0.58 ± 0.10	0.80 ± 0.10	0.36 ± 0.08	0.41 ± 0.08	**0.79 ± 0.14**
Val95Ala	strand 6	0.34 ± 0.08	0.57 ± 0.08	0.79 ± 0.08	0.38 ± 0.12	0.48 ± 0.12	**0.86 ± 0.15**
Phe97Ala	strand 6	0.55 ± 0.11	0.70 ± 0.11	0.85 ± 0.11	0.21 ± 0.04	**0.63 ± 0.07**	**0.92 ± 0.06**
Tyr108Ala	strand 7	0.50 ± 0.10	0.70 ± 0.10	0.87 ± 0.10	0.33 ± 0.04	0.48 ± 0.06	**0.85 ± 0.08**
Phe110Ala	strand 7	0.31 ± 0.03	0.60 ± 0.03	0.89 ± 0.03	0.05 ± 0.02	0.26 ± 0.03	0.45 ± 0.03
Met121Ala	loop	0.26 ± 0.10	0.53 ± 0.10	0.81 ± 0.10	0.06 ± 0.03	0.06 ± 0.03[c]	0.07 ± 0.03[c]
Leu125Ala	strand 8	0.42 ± 0.10	0.67 ± 0.10	0.79 ± 0.10	0.36 ± 0.08	0.59 ± 0.10	**0.96 ± 0.15**
average		0.46 ± 0.14	0.65 ± 0.10	0.86 ± 0.07	0.25 ± 0.12	0.50 ± 0.15	0.76 ± 0.15

[a] The ϕ-values are calculated as $\phi = \Delta\Delta G^{\ddagger}(X)/\Delta\Delta G_U(X)$ ($\Delta\Delta G_U(X)$ and $\Delta\Delta G^{\ddagger}(X)$ defined in Table 1) at each specified GuHCl condition (X). The β-values are calculated according to eq 3 (Materials and Methods) at each (X) value; errors are based on the accuracy in polynomial fits. For clarity, the ϕ-values that are above 0.6 are given in bold. [b] Standard deviations (σ) for the ϕ-values were calculated as in ref *7*: $\sigma_\phi = |\phi| \cdot \sqrt{[(\sigma_{\Delta\Delta G^{\ddagger}}/\Delta\Delta G^{\ddagger})^2 + (\sigma_{\Delta\Delta GU}/\Delta\Delta \mathbf{G}_U)^2]}$. [c] Not included in ϕ(average) calculations.

$= -c_U$ in eq 1 in Materials and Methods) which results in constant values of m_{F-U} ($= m_U - m_F$). In Figure 2A, the Tanford β-value derived for wild-type zinc-substituted azurin is plotted as a function of GuHCl concentration. This plot clearly shows that the transition state moves gradually from $\beta = 0.4$ in 0 M GuHCl (i.e., transition-state lies closer to the unfolded state in terms of hydrophobic-surface exposure) to $\beta = 0.9$ in 7 M GuHCl (i.e., transition state lies closer to the folded state in terms of hydrophobic-surface exposure). Similar movements occur for all the mutants (Table 2).

We used the movement of the transition state to reconstruct the shape of the folding free-energy profiles for zinc-substituted wild-type azurin at different GuHCl concentrations as outlined by Oliveberg in ref *25*. In short, wild-type zinc-substituted azurin's Chevron plot was first re-plotted as a function of β using the relation $\beta = 0.41 + 0.08$[GuHCl] (eq 3 in Materials and Methods; derived from polynomial fit parameters). Next, the barrier height (U − ‡) at each point of β was approximated as $\Delta G^{\ddagger} = RT(\ln 10^6 - \ln k_F)$, where the pre-factor of 10^6 s^{-1} is from ref *49*. However, the absolute value of this factor does not affect the general shape of the broad barrier. In the unfolding region, k_F was first obtained from k_U and the stability at each condition assuming a two-state relation. Finally, all points in the free-energy profile were extrapolated to a common [GuHCl]. Since β is a linear function of [GuHCl], each value of $\Delta G^{\ddagger}$ can be extrapolated to a common [GuHCl] (Y) by standard linear free-energy relations: $\Delta G^{\ddagger}(\beta,[Y]) = \Delta G^{\ddagger}(\beta,[X]) + \beta \cdot m_{F-U} \cdot RT([Y] - [X])$, where [X] is the GuHCl concentration at which $\ln k_F$ is measured. In Figure 2B, we show the resulting free-energy profiles as a function of β at 0, 2, 4, and 8 M GuHCl. The data clearly illustrates how zinc-substituted azurin's transition state (the highest point) moves along the top of a broad barrier as [GuHCl] is increased.

Residue-Specific Resolution of the Moving Folding Nucleus. Next, we used ϕ-value analysis to obtain information about the involvement of the mutated residues in the moving folding-transition state characteristic of zinc-substituted azurin. By measuring the change in protein stability, $\Delta\Delta G_U$,

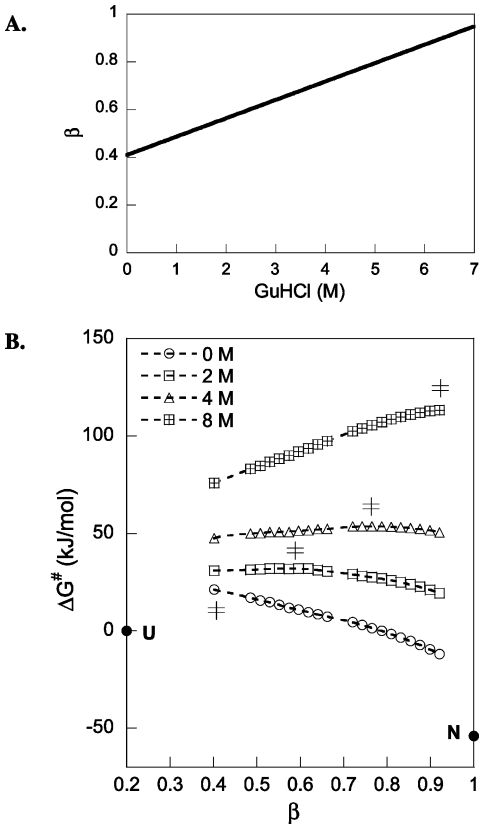

FIGURE 2: (A) The gradual change in the β-value as a function of GuHCl concentration for wild-type zinc-substituted azurin. (B) The shape of wild-type zinc-substituted azurin's folding free-energy profile as a function of the β-value (see text for details). The data illustrates how the highest point (the folding-transition state; indicated with (‡) moves along the top of a broad barrier as the GuHCl concentration is increased. The free-energy values for unfolded ($\beta = 0$) and folded ($\beta = 1$) zinc-substituted azurin at 0 M GuHCl are also shown (filled circles).

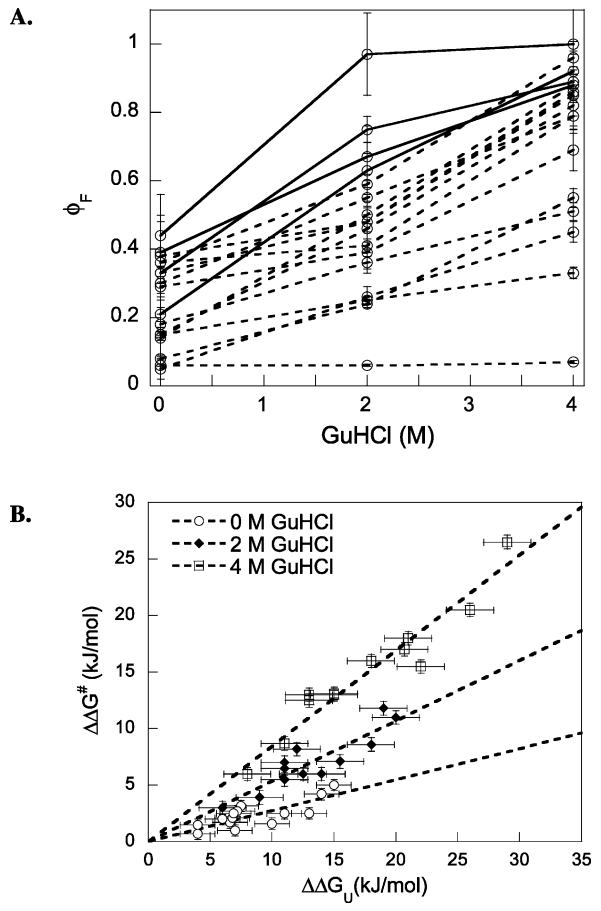

FIGURE 3: (A) ϕ-values as a function of GuHCl concentration for the zinc-substituted azurin variants (Table 2). Standard deviations in the ϕ-values are shown. Solid connecting lines correspond to Val31, Leu50, Ile81, and Phe97 data points. (B) Brønsted analysis of the effects of azurin mutations. Plot shows $\Delta\Delta G^{\ddagger}(X)$ versus $\Delta\Delta G_U(X)$ for 14 of the 17 positions studied at X = 0 (circles), 2 (diamonds), and 4 (squares) M GuHCl, respectively. Data points for Ile7, Phe110, and Met121 (all [GuHCl]) and Val5 at 2 and 4 M GuHCl, Val60 at 4 M GuHCl, and Leu50 at 2 M GuHCl are clear outliers and were excluded from this analysis. The slopes of the linear fits to each set of data result in $\phi_{av} = 0.27$ ($R = 0.78$; 0 M GuHCl), $\phi_{av} = 0.53$ ($R = 0.90$; 2 M GuHCl), and $\phi_{av} = 0.85$ ($R = 0.96$; 4 M GuHCl). Standard deviations are shown in both dimensions.

and the change in folding barrier (i.e., folding speed; $\Delta\Delta G^{\ddagger}$) due to mutation of a particular residue, we calculated the ϕ-value for that residue as $\phi = \Delta\Delta G^{\ddagger}/\Delta\Delta G_U$ (see definitions in legends to tables). The ϕ values derived for the 17 mutated positions in azurin are given in Table 2, at three selected GuHCl concentrations (0, 2, and 4 M GuHCl). The average ϕ-value gradually increases from 0.25 (0 M GuHCl, $\beta_{av} = 0.46$) to 0.50 (2 M GuHCl, $\beta_{av} = 0.65$) to 0.76 (4 M GuHCl, $\beta_{av} = 0.86$) (Figure 3A). Upon comparing ϕ_{av} and β_{av}, the average β-value is somewhat larger than the average ϕ-value at each condition (Table 2). This is reasonable since chain compaction and burial of exposed hydrophobic surface area, as reported on by β-values, do not necessarily require specific side-chain interactions, which is given by the ϕ-values.

The gradual increase of native-like structure in the transition state can also be illustrated in a Brønsted plot (Figure 3B) (*37*). The presence of linear dependences between correlating $\Delta\Delta G^{\ddagger}$ and $\Delta\Delta G_U$ values implies that most investigated positions participate in a diffuse folding nucleus. The slopes of such linear fits correspond to the average ϕ-value for each [GuHCl]/β condition. The clear trend of increasing ϕ_{av} as a function of GuHCl (slopes of 0.27 for 0 M, 0.53 for 2 M, and 0.85 for 4 M GuHCl data) demonstrates that the probed residues' interactions become more native-like as the β-value increases. Detailed inspection of the individual ϕ-values at the three selected conditions (Figure 3A, Table 2) reveals a significant spread. This heterogeneity is used to determine where the diffuse folding nucleus initiates and how structure is then propagated among the probed residues as the nucleus grows more and more native-like (see Discussion).

DISCUSSION

Few proteins have been reported to fold by two-state kinetics and exhibit moving-transition states (*21*, *22*). To date, analysis of this behavior with residue-specific resolution has only been reported for the 102-residue protein U1A (*25*) and for CI2 (*21*). Nonetheless, this behavior presents a rare opportunity to experimentally observe new regions of free-energy profiles for protein folding. Zinc-substituted *P. aeruginosa* azurin is the largest protein reported to folds via a two-state kinetic reaction that involves a moving folding-transition state (*38*, *45*).

We note that there are many origins of curved Chevron plots (see Introduction), and care must be taken upon interpretation. For zinc-substituted azurin, we exclude transient aggregation (based on the lack of protein-concentration dependence in the kinetics), transient intermediates (since there is no missing amplitude either by CD or fluorescence in the stopped-flow kinetics), and ground-state effects (since wild-type and all mutant zinc-variants exhibit similar, and constant in the denaturant range tested, m_{F-U} values). Moreover, switches between parallel pathways are excluded since then there would be an upward curvature, and most often only in one of the two limbs (*21*, *22*). Recently, moving transition states were explained by a switch between a few consecutive narrow barriers on a sequential folding pathway (*20*, *50*). We disfavor this explanation for zinc-substituted azurin since in such cases the position of the transition state should change in a narrow range of denaturant concentrations but exhibit constant ϕ-values at higher and lower denaturant concentrations. Alternatively, if there are two distinct barriers separated by a high-energy meta-stable intermediate, this mechanism may result in a kink instead of curvature in the Chevron plot (*20*, *50*). In contrast, for all the zinc-substituted azurin variants, the curvature is smooth throughout the tested denaturant-concentration range and all proteins (including wild-type) display curvature; this behavior is best explained as a broad continuous transition-state barrier for folding (*20*, *25*).

Inspection of the individual ϕ-values for the 17 studied positions in zinc-substituted azurin (Figure 3A, Table 2) reveals a sequence of events for the development and consolidation of azurin's folding nucleus (Figure 4). Initially, partially formed interactions appear diffusively throughout the tested residues ($\phi_{av} \sim 0.25$; $\beta_{av} \sim 0.46$) with a leading density situated on the core residue Leu50 in strand 4 ($\phi \sim 0.44$; $\beta_{av} \sim 0.46$) that extends to Val31 in strand 3 and Val95 in strand 7 ($\phi \sim 0.4$ for both; $\beta_{av} \sim 0.46$). Notably, these three residues are facing each other in the hydrophobic core, and Leu50 and Val31 are in the same registry of the

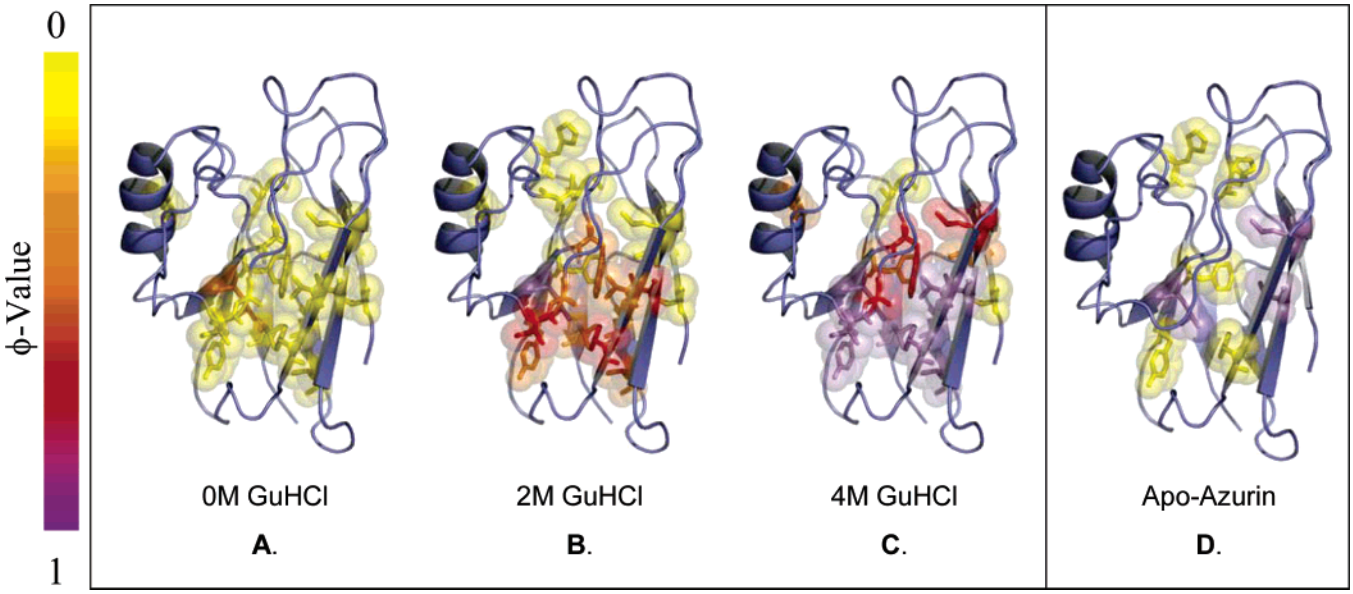

FIGURE 4: Snapshots of zinc-substituted azurin's folding nucleus at 0 (A), 2 (B), and 4 (C) M GuHCl, respectively. For comparison, apo-azurin's fixed folding-transition state is also shown (D). Probed residues are shown in space-filling and color-coded as follows: $\phi = 0-0.39$, yellow; $\phi = 0.4-0.59$, orange; $\phi = 0.6-0.79$, red; $\phi = 0.8-1.0$, purple. In B, the ϕ-value for the zinc-site (i.e., His117 and Cys112 side chains) is also included (see text for calculation). Structures were prepared using 1AZU and the program PyMol. B (zinc-form) and D (apo-form) figures show transition-state structures at similar β-values.

β-strands. Next, in a rather abrupt manner, native-like ($\phi \sim 1$; $\beta_{av} \sim 0.65$) structure appears around the Leu50 side chain. This implies that it may form interactions with residue 82 in strand 5 and residue 97 in strand 6 which are the closest interaction partners in the native-state based on 1AZU structural analysis. In agreement, the Phe97 side chain also becomes more structured at this point ($\phi \sim 0.63$; $\beta_{av} \sim 0.65$). The simultaneous increase in the ϕ-values for Val31 ($\phi \sim 0.7$; $\beta_{av} \sim 0.65$) and Ile81 ($\phi \sim 0.75$; $\beta_{av} \sim 0.65$) implies interactions between Val31 (strand 3) and Ile81 (strand 5) and residues in strands 4 (Leu50) and 6 (Phe97), which are all close-interaction partners according to 1AZU structural analysis. Next, this leads to a "zipping up" of strands 2, 4, 5, and 6 (i.e., native-like interactions for Ile20 and Val22 in strand 2, Trp48 and Leu50 in strand 4, Ile81 and Ala82 in strand 5, and Val95 and Val97 in strand 6) and consolidation with native structure around Tyr108 in strand 7, Val31 in strand 3, and Leu125 in strand 8. At this point, the folding nucleus can be considered large and well-structured ($\phi \sim 0.8-1$ for mentioned residues; $\beta_{av} \sim 0.86$). Phe110 (in strand 7), Leu33 (in strand 3), and Val60 (in the helix) appear to be on the edge of the structured core, since their interactions are not fully formed at these conditions ($\phi \sim 0.4-0.7$ at $\beta_{av} \sim 0.86$). Strand 1 (Val 5 and Ile7) as well as Met121 (which is in the loop between strands 7 and 8) interactions do not seem to participate in this highly structured core ($\phi \sim 0-0.5$ at $\beta_{av} \sim 0.86$). Taken together, folding begins around Leu50 with a diffuse delocalized nucleus (involving residues in four strands) which gradually grows, following a typical nucleation−condensation pattern, until a highly structured core is formed that involves most of β-strands 2, 4, 5, and 6 and parts of β-strands 3, 7, and 8 (Figure 4). To reach the folded state from here, one might imagine a simple "zipping up" of the remaining β-strand regions and the helix as well as establishment of loop−residue interactions. In U1A's moving transition state, the two initiation sites seemed to collapse more abruptly than the rest of the structure (*25*); this is also the case for azurin's initiation site, the side chain of Leu50 (Figure 3A), which acquires a ϕ of 1 straightaway at $\beta_{av} \sim 0.65$. This supports Oliveberg's hypothesis that abrupt collapse is a hallmark of conformationally restricted nucleation in mesophilic systems (*25*).

Details on the folding-transition state of *P. aeruginosa* apo-azurin was recently reported (*43*). Although the apo-form also displays two-state behavior, there is a marked difference in the kinetics. Apo-azurin exhibits a classical V-shaped Chevron with a β-value of ~0.6 throughout. Of the six positions in apo-azurin for which reliable ϕ-values were reported, three formed native-like interactions in the folding-transition state ($\phi_{av} \sim 0.98$ for Leu50, Val31, Leu33), whereas the other three did not participate as significantly in the folding nucleus ($\phi_{av} \sim 0.24$ for Phe97, Phe108, Leu110). Moreover, earlier folding work on apo-azurin reported $\phi < 0.2$ for His117 and His 46 side chains (*37*). Apo-azurin's folding-transition state thus appears to belong to the "polarized" class as opposed to the "diffuse" class discussed in the Introduction (Figure 4D). Interestingly, the residues with high ϕ-values contributed little to the overall thermodynamic stability of apo-azurin, whereas the residues with low ϕ-values had large effects on $\Delta G_U(H_2O)$. The residues probed in apo-azurin had earlier been reported to be structural determinants since they are conserved across all or most sandwich-like proteins (*42*). Our observations allowed us to propose mutually exclusive roles for these residues in guiding the folding reaction and governing structural stability (*43*). The anticipated roles for these conserved residues may still hold true for most members of the sandwich-like protein family since most of these proteins do not coordinate cofactors. In vivo, the azurin polypeptide likely folds in the apo-form, although we have speculated that copper may be incorporated before polypeptide folding (*36*). The zinc-form of azurin is not biologically active and it is not present in *P. aeruginosa* (*34*).

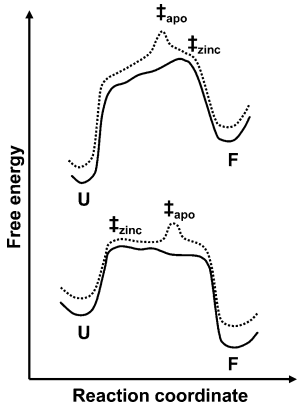

FIGURE 5: Illustration showing an activation barrier that unifies the kinetic behaviors of apo- and zinc-forms of azurin. A small hilltop in apo-azurin's free-energy profile (dotted curve) may account for its fixed transition state ($‡_{apo}$). Suppression of this feature by the presence of zinc reveals the underlying smooth and broad activation barrier (solid curve); this results in a moving transition state ($‡_{zinc}$) for zinc-substituted azurin. Strongly denaturing conditions, top; native-like conditions, bottom.

Despite zinc-azurin's apparent lack of biological relevance, it is remarkable from a fundamental physical view that the presence of zinc has such a drastic effect on azurin's kinetic folding behavior. The only difference between apo- and zinc-forms of azurin is the presence of zinc coordinating to two residues in the unfolded polypeptide (His117 and Cys112). However, earlier work on the two-state folding proteins S6 and CI2 showed that several point mutations altered the V-shaped Chevron plot to the curved variety. Thus, in these two proteins, point-mutations were able to change fixed folding nuclei to ones that move as a function of denaturant (*23*). The kinetic differences were explained by relatively small alterations on a *common* free-energy profile; apparent sharp activation barriers are the result of small hilltops in generally flat and broad activation barriers. It was proposed that broad activation barriers are a unifying feature of two-state folding that can account for a range of different folding behaviors (*24*). Applied to azurin, it implies that the fixed transition state for apo-azurin is the result of a small pointed feature projecting from the top of an otherwise broad free-energy profile (Figure 5). The presence of zinc in the unfolded state suppresses this local bump, and the broad activation barrier becomes accessible. The lack of unique energetically elevated features in this broad free-energy profile results in the moving transition state that is observed for zinc-substituted azurin. The free-energy profiles in Figure 2B clearly demonstrate zinc-azurin's smooth and broad activation barrier. Only a few kilocalories per mol may separate fixed and moving transition states (*24*). Likewise, the zinc interaction with Cys112 and His117 in unfolded azurin corresponds to a free energy of roughly 7 kcal/mol (*45*), which is more than sufficient to alter the shape of the activation barrier (i.e., suppress a local hilltop).

Although not strictly correct, we can use the stability and kinetic data for apo- and zinc-forms of azurin at conditions that exhibit similar β-values to derive an apparent ϕ-value for the zinc-site (i.e., wild-type apo-azurin as "mutant", wild-type zinc-substituted azurin as "wild-type"). The β-value for folding of apo-azurin is 0.6 (*37*, *43*). Since $\beta = 0.58$ for wild-type zinc-substituted azurin in 2 M GuHCl (Table 2), we used data at this condition (2 M GuHCl, pH 7, 25 °C) to estimate a ϕ of 0.33 ± 0.04 ($= (RT \ln[k_F(\text{apo-azurin})/(k_U(\text{zinc-azurin})])/[\Delta G_U(\text{apo-azurin}) - \Delta G_U(\text{zinc-azurin})]$) for the zinc-site. This result demonstrates that zinc-azurin's diffuse transition state extends to the zinc-site. The two unfolded-state zinc ligands, Cys112 and His117, are situated toward the C-terminus in a loop region between β-strands 7 and 8. In agreement, Met121 (probed in this work) is positioned at the edge of this loop and also has a low ϕ-value. Intriguingly, the rather low ϕ-value for the zinc-site underscores that albeit the presence of zinc alters the folding free-energy landscape, the zinc site does not direct the folding process.

CONCLUSIONS

Here we take advantage of zinc-substituted *P. aeruginosa* azurin's dynamic folding-transition state to obtain snapshots, with residue-specific resolution, of the growing folding nucleus. It emerges that the transition-state is diffuse and grows gradually, in a nucleation−condensation manner, around a center density on the core residue Leu50. Azurin, with its 128 residues, is the largest two-state folding protein shown to exhibit a moving transition-state. In contrast to the zinc-form, apo-azurin folds via a fixed folding-transition state. This difference in behavior emphasizes that folding barriers for two-state folding proteins are generally broad and that localized transition states result from minor pointed features in the free-energy profiles.

ACKNOWLEDGMENT

We thank Jessica Marks (Tulane University, New Orleans, LA) for creating some azurin variants on the DNA level.

SUPPORTING INFORMATION AVAILABLE

Figures that show observed fluorescence signals at 308 nm versus GuHCl concentration for all variants (S1) and tables that list natural logarithms of observed rate constants versus GuHCl concentration for all variants (S2). This material is available free of charge via the Internet at http://pubs.acs.org.

REFERENCES

1. Jackson, S. E. (1998) How do small single-domain proteins fold? *Folding Des. 3*, R81−91.
2. Kamagata, K., Arai, M., and Kuwajima, K. (2004) Unification of the folding mechanisms of non-two-state and two-state proteins, *J. Mol. Biol. 339*, 951−965.
3. Lindorff-Larsen, K., Vendruscolo, M., Paci, E., and Dobson, C. M. (2004) Transition states for protein folding have native topologies despite high structural variability, *Nat. Struct. Mol. Biol. 11*, 443−449.
4. Matouschek, A., Kellis, J. T., Jr., Serrano, L., Bycroft, M., and Fersht, A. R. (1990) Transient folding intermediates characterized by protein engineering, *Nature 346*, 440−445.
5. Matouschek, A., and Fersht, A. R. (1991) Protein engineering in analysis of protein folding pathways and stability, *Methods Enzymol. 202*, 82−112.
6. Fersht, A. R., and Sato, S. (2004) Phi-value analysis and the nature of protein-folding transition states, *Proc. Natl. Acad. Sci. U.S.A. 101*, 7976−7981.
7. Sanchez, I. E., and Kiefhaber, T. (2003) Origin of unusual phi-values in protein folding: evidence against specific nucleation sites, *J. Mol. Biol. 334*, 1077−1085.
8. Goldenberg, D. P. (1999) Finding the right fold, *Nat. Struct. Biol. 6*, 987−990.
9. Itzhaki, L. S., Otzen, D. E., and Fersht, A. R. (1995) The structure of the transition state for folding of chymotrypsin inhibitor 2

analysed by protein engineering methods: evidence for a nucleation-condensation mechanism for protein folding, *J. Mol. Biol. 254*, 260−288.
10. Milla, M. E., Brown, B. M., Waldburger, C. D., and Sauer, R. T. (1995) P22 Arc repressor: transition state properties inferred from mutational effects on the rates of protein unfolding and refolding, *Biochemistry 34*, 13914−13919.
11. Lopez-Hernandez, E., and Serrano, L. (1996) Structure of the transition state for folding of the 129 aa protein CheY resembles that of a smaller protein, CI-2, *Folding Des. 1*, 43−55.
12. Burton, R. E., Huang, G. S., Daugherty, M. A., Calderone, T. L., and Oas, T. G. (1997) The energy landscape of a fast-folding protein mapped by Ala → Gly substitutions, *Nat. Struct. Biol. 4*, 305−310.
13. Kragelund, B. B., Osmark, P., Neergaard, T. B., Schiodt, J., Kristiansen, K., Knudsen, J., and Poulsen, F. M. (1999) The formation of a native-like structure containing eight conserved hydrophobic residues is rate limiting in two-state protein folding of ACBP, *Nat. Struct. Biol. 6*, 594−601.
14. Northey, J. G., Di Nardo, A. A., and Davidson, A. R. (2002) Hydrophobic core packing in the SH3 domain folding transition state, *Nat. Struct. Biol. 9*, 126−130.
15. Capaldi, A. P., Kleanthous, C., and Radford, S. E. (2002) Im7 folding mechanism: misfolding on a path to the native state, *Nat. Struct. Biol. 9*, 209−216.
16. Kim, D. E., Fisher, C., and Baker, D. (2000) A breakdown of symmetry in the folding transition state of protein L, *J. Mol. Biol. 298*, 971−984.
17. Riddle, D. S., Grantcharova, V. P., Santiago, J. V., Alm, E., Ruczinski, I., and Baker, D. (1999) Experiment and theory highlight role of native state topology in SH3 folding, *Nat. Struct. Biol. 6*, 1016−1024.
18. Tanford, C. (1968) Protein denaturation, *Adv. Protein Chem. 23*, 121−282.
19. Tanford, C. (1970) Protein denaturation. C. Theoretical models for the mechanism of denaturation. *Adv Protein Chem. 24*, 1−95.
20. Sanchez, I. E., and Kiefhaber, T. (2003) Evidence for sequential barriers and obligatory intermediates in apparent two-state protein folding, *J. Mol. Biol. 325*, 367−376.
21. Sanchez, I. E., and Kiefhaber, T. (2003) Hammond behavior versus ground-state effects in protein folding: evidence for narrow free energy barriers and residual structure in unfolded states, *J. Mol. Biol. 327*, 867−884.
22. Sanchez, I. E., and Kiefhaber, T. (2003) Non-linear rate-equilibrium free energy relationships and Hammond behavior in protein folding, *Biophys. Chem. 100*, 397−407.
23. Oliveberg, M., Tan, Y. J., Silow, M., and Fersht, A. R. (1998) The changing nature of the protein folding transition state: implications for the shape of the free-energy profile for folding, *J. Mol. Biol. 277*, 933−943.
24. Otzen, D. E., Kristensen, O., Proctor, M., and Oliveberg, M. (1999) Structural changes in the transition state of protein folding: alternative interpretations of curved chevron plots, *Biochemistry 38*, 6499−6511.
25. Ternstrom, T., Mayor, U., Akke, M., and Oliveberg, M. (1999) From snapshot to movie: phi analysis of protein folding transition states taken one step further, *Proc. Natl. Acad. Sci. U.S.A. 96*, 14854−14859.
26. Oliveberg, M. (2001) Characterisation of the transition states for protein folding: towards a new level of mechanistic detail in protein engineering analysis, *Curr. Opin. Struct. Biol. 11*, 94−100.
27. Bryngelson, J. D., Onuchic, J. N., Socci, N. D., and Wolynes, P. G. (1995) Funnels, pathways, and the energy landscape of protein folding: a synthesis, *Proteins 21*, 167−195.
28. Finkelstein, A. V., and Badretdinov, A. (1997) Rate of protein folding near the point of thermodynamic equilibrium between the coil and the most stable chain fold, *Folding Des. 2*, 115−121.
29. Pande, V. S., Grosberg, A., and Tanaka, T. (1997) On the theory of folding kinetics for short proteins, *Folding Des. 2*, 109−114.
30. Sali, A., Shakhnovich, E., and Karplus, M. (1994) How does a protein fold? *Nature 369*, 248−251.
31. Silow, M., and Oliveberg, M. (1997) High-energy channeling in protein folding, *Biochemistry 36*, 7633−7637.
32. Adman, E. T. (1991) Copper protein structures, *Adv. Protein Chem. 42*, 145−197.
33. Nar, H., Messerschmidt, A., Huber, R., van de Kamp, M., and Canters, G. W. (1992) Crystal structure of *Pseudomonas aeruginosa* apo-azurin at 1.85 Å resolution, *FEBS Lett. 306*, 119−124.
34. Nar, H., Huber, R., Messerschmidt, A., Filippou, A. C., Barth, M., Jaquinod, M., van de Kamp, M., and Canters, G. W. (1992) Characterization and crystal structure of zinc azurin, a by-product of heterologous expression in *Escherichia coli* of *Pseudomonas aeruginosa* copper azurin, *Eur. J. Biochem. 205*, 1123−1129.
35. Pozdnyakova, I., Guidry, J., and Wittung-Stafshede, P. (2001) Copper stabilizes azurin by decreasing the unfolding rate, *Arch. Biochem. Biophys. 390*, 146−148.
36. Pozdnyakova, I., and Wittung-Stafshede, P. (2001) Copper binding before polypeptide folding speeds up formation of active (holo) *Pseudomonas aeruginosa* azurin, *Biochemistry 40*, 13728−13733.
37. Pozdnyakova, I., Guidry, J., and Wittung-Stafshede, P. (2002) Studies of *Pseudomonas aeruginosa* azurin mutants: cavities in beta-barrel do not affect refolding speed, *Biophys. J. 82*, 2645−2651.
38. Pozdnyakova, I., and Wittung-Stafshede, P. (2003) Approaching the speed limit for Greek Key beta-barrel formation: transition-state movement tunes folding rate of zinc-substituted azurin, *Biochim. Biophys. Acta 1651*, 1−4.
39. Fuentes, L., Oyola, J., Fernandez, M., and Quinones, E. (2004) Conformational changes in azurin from *Pseudomona aeruginosa* induced through chemical and physical protocols, *Biophys. J. 87*, 1873−1880.
40. Pozdnyakova, I., and Wittung-Stafshede, P. (2001) Biological relevance of metal binding before protein folding, *J. Am. Chem. Soc. 123*, 10135−10136.
41. Wittung-Stafshede, P. (2004) Role of cofactors in folding of the blue-copper protein azurin, *Inorg. Chem. 43*, 7926−7933.
42. Kister, A. E., Finkelstein, A. V., and Gelfand, I. M. (2002) Common features in structures and sequences of sandwich-like proteins, *Proc. Natl. Acad. Sci. U.S.A. 99*, 14137−14141.
43. Wilson, C. J., and Wittung-Stafshede, P. (2005) Role of structural determinants in folding of the sandwich-like protein *Pseudomonas aeruginosa* azurin, *Proc. Natl. Acad. Sci. U.S.A. 102*, 3984−3987.
44. Wittung-Stafshede, P. (2002) Role of cofactors in protein folding, *Acc. Chem. Res. 35*, 201−208.
45. Marks, J., Pozdnyakova, I., Guidry, J., and Wittung-Stafshede, P. (2004) Methionine-121 coordination determines metal specificity in unfolded *Pseudomonas aeruginosa* azurin, *J. Biol. Inorg. Chem. 9*, 281−288.
46. Fersht, A. (1999) *Structure and Mechanism in Protein Science*, W. H. Freeman and Company, New York.
47. Pace, C. N., and Shaw, K. L. (2000) Linear extrapolation method of analyzing solvent denaturation curves, *Proteins* (Suppl. 4), 1−7.
48. Mei, G., Di Venere, A., Campeggi, F. M., Gilardi, G., Rosato, N., De Matteis, F., and Finazzi-Agro, A. (1999) The effect of pressure and guanidine hydrochloride on azurins mutated in the hydrophobic core, *Eur. J. Biochem. 265*, 619−26.
49. Jones, C. M., Henry, E. R., Hu, Y., Chan, C. K., Luck, S. D., Bhuyan, A., Roder, H., Hofrichter, J., and Eaton, W. A. (1993) Fast events in protein folding initiated by nanosecond laser photolysis, *Proc. Natl. Acad. Sci. U.S.A. 90*, 11860−11864.
50. Bachmann, A., and Kiefhaber, T. (2001) Apparent two-state tendamistat folding is a sequential process along a defined route, *J. Mol. Biol. 306*, 375−386.

BI050342N